ELSEVIER

Journal of Fluids and Structures 19 (2004) 73–92

JOURNAL OF FLUIDS AND STRUCTURES

www.elsevier.nl/locate/jnlabr/yjfls

Vortex induced vibrations using Large Eddy Simulation at a moderate Reynolds number

H. Al-Jamal, C. Dalton*

Mechanical Engineering Department, University of Houston, Houston, TX 77204-4006, USA

Received 13 November 2002; accepted 8 October 2003

Abstract

This paper presents the results of a computational study on the vortex-induced vibration of a circular cylinder. We have performed a 2-D LES study of the VIV response of a circular cylinder at a Reynolds number of 8000 with a range of damping ratios and natural frequencies. A combined Dirichlet–Neumann outflow boundary condition was used to allow the wake vortices to pass through the outflow boundary, undisturbed by the boundary. In spite of the shortcomings of a 2-D representation, the results show the expected vibratory response of the cylinder for $0.555 < f_{so}/f_N < 1.59$, where f_{so} is the nonvibrating vortex-shedding frequency and f_N is the natural frequency. For a solid cylinder with a mass factor (m^*) of 7.85 and a material-damping ratio of 0.02, lock-on was observed for $0.793 < f_{so}/f_N < 1.39$ with a peak at a reduced velocity of 5.5. Decreasing the value of material damping had the effect of increasing the extent of the lock-on range. A beating behavior in the oscillation was observed which diminished considerably as the damping value was increased. A decrease in the mass factor to 1.67 caused the lock-on range to broaden considerably as a function of reduced velocity. In addition, the amplitude of oscillation increased by a factor of almost three for the lower value of mass factor. The standard 2S, 2P, etc. vortex structures observed at low Reynolds numbers for sinusoidal oscillations were not found in this self-excited case. Several reasons are suggested for this particular lack of agreement with some previous results. These results are seen to represent the VIV behavior of a cylinder reasonably well for the parameter values used in these calculations.

1. Introduction

A circular cylinder, subject to a flowing fluid, has a tendency to vibrate under certain conditions. The vibration can be transverse to the direction of the flow, in-line with the direction of the flow, or a combination of the two. This vortex-induced vibration (VIV) occurs when the vortex-shedding frequency and the cylinder natural frequency are properly matched. Prediction of this self-excited vibration has been a challenge to fluid mechanicians and offshore designers for many years. The focus in this study will be on the calculation of the VIV problem.

One of the difficulties in considering this problem is that the flow field behind a stationary cylinder is quite different from that behind an oscillating cylinder. The stationary (or fixed) cylinder has been the subject of numerous studies, both experimental and computational, for many years. As a result, the fixed-cylinder problem is relatively well understood regarding the wake behavior and its vorticity dynamics. However, when the vortex-shedding frequency approaches the cylinder natural frequency, the vortex shedding frequency becomes synonymous with the natural frequency and the cylinder begins to vibrate in the transverse direction. This is the classical vortex-induced vibration (VIV) problem. As soon as the vibration begins, the flow field behind the cylinder (the wake flow) becomes more

*Corresponding author.
E-mail address: dalton@uh.edu (C. Dalton).

0889-9746/$ - see front matter © 2003 Elsevier Ltd. All rights reserved.
doi:10.1016/j.jfluidstructs.2003.10.005

complex and the calculation of the flow field becomes more difficult because the cylinder is now moving. The cylinder motion affects the time-dependent pressure and shear stress distributions; hence, the self-excitation forcing function for vibratory motion of the cylinder is different from the transverse-direction forcing function for a stationary cylinder. In vibratory motion, the flow field and the forcing function are both quite time dependent and the cylinder motion is coupled to the fluid forcing function in a way that requires the flow field and cylinder displacement to be calculated simultaneously. Parameters influencing this problem are the mass of the cylinder relative to the mass of the displaced fluid (the mass factor), the Reynolds number of the flow for the cylinder at rest, and the material damping and structural stiffness values of the oscillating cylinder.

The shedding of vortices, alternately and periodically, from a stationary circular cylinder is not perfectly correlated in the spanwise direction. In the Reynolds number range of $10^4 < \mathrm{Re} < 10^5$, the correlation length is from three to six cylinder diameters (see Sarpkaya, 1979). However, when the cylinder begins to oscillate, the vortex structure is significantly altered. The flow between adjacent axial segments of the cylinder becomes coupled and the correlation length for vortex shedding increases noticeably. Thus, once oscillation has begun, it is enhanced by the alteration of the shedding pattern toward a conventional 2-D structure. Bearman (1984) notes that there is a threshold oscillation magnitude beyond which the correlation length experiences a significant increase. For a circular cylinder, the critical value of oscillation is $y/D = 0.05$ which is quite small for VIV oscillations.

The true VIV problem is where the cylinder motion is self-excited by the flow at the location of the cylinder, i.e., there is feedback between the fluid flow and the cylinder motion. Due to complexities in describing the coupling between motion and force, there are many studies that provide a representation of a slightly different problem. This companion problem, known as the forced-vibration problem, is when the cylinder is forcibly oscillated at a specified frequency and amplitude and the resulting fluid motion and force description are obtained. The numerous forced-oscillation studies will not be considered in this study.

In this effort, the self-excited vibration problem will be addressed from a computational viewpoint. At the present time, there have been several different computational approaches toward describing the flow field for this problem. These include the discrete-vortex method, direct numerical simulation (DNS), Reynolds-averaged Navier–Stokes (RANS), Large Eddy Simulation (LES), and combinations of the four. Recent studies in the self-excited vibration (VIV) problem include those by Saltara et al. (1998), who did a combination discrete-vortex/LES study at $\mathrm{Re} = 1000$ for a one degree of freedom (DOF) problem (transverse direction); Zhou et al. (1999), who used the vortex-in-cell (VIC) method at $\mathrm{Re} = 200$ for a two-DOF problem; Evangelinos et al. (2000), who did a 3-D DNS study (1-DOF) at $\mathrm{Re} = 1000$ for flexible cylinders; and Guilmineau and Queutey (2001) who did a 2-D finite-volume study (1-DOF) of cylinder oscillation for Re in the range 900–15 000. Tutar and Holdo (2000) did a 3-D finite-element/LES study on the forced oscillation of cylinders at $\mathrm{Re} = 2.4 \times 10^4$.

LES solutions of the problem of a steady flow past a stationary circular cylinder are thought to be the most accurate of the calculation methods for Reynolds numbers which exceed the present DNS capability. This issue has been discussed by Majumdar and Rodi (1985), Lu et al. (1997), and Tutar and Holdo (2000). Among the most recent LES solutions for a steady approach flow are those of Lu et al. (1997), Jordan and Ragab (1998), Breuer (1999), Kravchenko and Moin (2000) (all for fixed cylinders), and Tutar and Holdo (2000) (for the forced oscillation of a cylinder).

The natural approach to a prediction of VIV in self-excited vibration is a method that couples the fluid motion and the motion of the cylinder. This coupled approach has been taken by most of the recent investigations into the VIV problem. Extension to a 3-D structural description is most reasonable when the strip theory approach is used, as discussed by Dalheim (1999), Herjford et al. (1999), and Yamamoto et al. (2001). This is a solution method wherein a very long cylinder is divided into segments or "strips" along its length. Each strip is then treated as an individual cylinder for 2-D or 3-D flow calculations and then the complete cylinder is reconstructed by re-assembling the segments. There is some obvious inexactness in doing this because of the phase differences that will exist between the segments.

The second author's previous VIV studies have used the coupled fluids/structure approach in describing the problem and using LES up to $\mathrm{Re} = 13\,000$. Zhang and Dalton (1997) and Lu and Dalton (1996) examined the VIV problem for 2-D viscous flow at $\mathrm{Re} = 200$ and 2-D turbulent flow (using LES) at $\mathrm{Re} = 855$ and compared the results to those of Ongoren and Rockwell (1988), Lecointe and Piquet (1989), and Gu et al. (1994). Very good agreement was found with the Ongoren and Rockwell results and reasonably good agreement with the results of Lecointe and Piquet where the lack of agreement was in the lift coefficient result. The lift calculations of Lecointe and Piquet, who used no turbulence modelling, were about 35% higher at $\mathrm{Re} = 855$ than those of Zhang and Dalton (1997). In a similar study preceding the present effort, Zhang and Dalton (1996) undertook a 2-D LES study for a transversely oscillating cylinder at $\mathrm{Re} = 13\,000$. An amplitude-to-diameter oscillation of about 0.26, with damping ratio of 0.02, was obtained and lock-on was observed to occur from f_{so}/f_N of about 1.0 to 1.3, where f_{so} is the stationary cylinder vortex-shedding frequency and f_N is the natural frequency. These results showed the same trends as the experimental results of Feng (1968) who undertook one of the first comprehensive experimental studies of this problem. However, the results of Zhang and

Dalton (1996) did not provide the kind of agreement necessary for full confidence in the calculation method. Another study on the VIV problem is that of Tutar and Holdo (2000) who used a 3-D LES finite-element approach to examine the forced-oscillation case at $Re = 2.4 \times 10^4$. Tutar and Holdo found that the 3-D representation was necessary to get accurate results when the cylinder is vibrating. It is well known that, for a fixed cylinder, a 2-D calculation produces a drag coefficient that is 5–10% too large for Reynolds numbers up to several thousand. The absence of the 3-D effects in the wake causes the base pressure to be more negative which leads to an increase in the drag coefficient. A major cause of the higher drag coefficient is the perfect spanwise correlation of the shed vortices that is inherent in the 2-D representation. At higher values of Re, the trend of higher 2-D drag coefficients continue, but the trend is not as regular as at the lower values of Re. There is not yet universal agreement on the reason for the irregular behavior in the value of $\bar{C}_D$ at higher Reynolds numbers. However, the reason seems to be the inadequacy of any 2-D turbulence model (in our case, LES) to capture the wake effects properly. This issue will be raised again when the results of our calculations are presented. Not surprisingly, Tutar and Holdo have found that the 3-D results for the forced oscillation of a cylinder provided better agreement with experimental data than were obtained for 2-D calculations. Even so, the 2-D representation of VIV should be reasonably accurate because of the increased spanwise correlation of the wake vortices when oscillation begins. Guilmineau and Queutey (2001) used a 2-D $k-\omega$ RANS solution to represent the flow past a cylinder with low mass-damping. The calculated results were compared to the experimental results of Khalak and Williamson (1999) over the range of Re from 900 to 15 000. The results correctly predict the maximum amplitude of oscillation, but the lower oscillation branch is not matched very well by Guilmineau and Queutey.

We recognize that a 2-D calculation is not truly representative of a turbulent flow. In addition, we recognize that even a 3-D turbulence model is inadequate to capture the full effects of the flow. Clearly, the 2-D approach is not going to capture any 3-D effects in the wake which means that base pressure will be more negative in the 2-D approach than in 3-D. But even beyond this shortcoming, a full 3-D LES model is incapable of modelling the transition that occurs in the wake and in the shear layers and, especially, the boundary layer. (In saying this, we recognize that our Reynolds number ($Re = 8000$) certainly is not large enough for the boundary layer on the cylinder to be turbulent.) These processes are too complicated and, perhaps, each is not well enough understood in its own right to be modelled properly, especially by a single technique such as LES. Thus, an LES model, either 2-D or 3-D, is not capable of calculating the full flow past a stationary cylinder, much less an oscillating one. This statement is not intended to be an indictment of the LES model because the same statement is true for virtually any turbulence model. The only method capable of capturing all of the aspects of turbulence is the method of DNS and present-day computers are not ready for the challenge of a high Reynolds number calculation for the kinds of flows discussed herein.

However, a 2-D calculation does allow for a reasonably accurate estimate of global parameters such as the drag and lift coefficients, especially when VIV begins because the wake correlation length increases significantly when VIV is established. The negative aspect of doing a 2-D calculation is that the influence of the spanwise wake turbulence is omitted. At Reynolds numbers in the laminar wake regime ($Re \approx 200$), the 2-D calculation overpredicts the drag coefficient up to 10%. At higher values of Re (such as $Re = 8000$ or 13 000), overprediction still occurs, but the overprediction trend is not quite as clear. When the cylinder is oscillating, the 2-D representation is more realistic than when the cylinder is stationary. Transverse oscillation of the cylinder causes the correlation length of the wake vortices to increase which diminishes the 3-D influence of vortex shedding. The authors are unaware of any study, which examines the difference between 2-D and 3-D calculations for an oscillating cylinder. The lift coefficient is also overpredicted in the 2-D representation, but an understanding of the amount of overprediction is not as well established as that of the drag coefficient.

However, at Reynolds numbers with significant wake turbulence, the vortex-shedding behavior does show some difference between the 2-D and 3-D calculations. The 2-D approach is not expected to provide a noticeable difference from the actual 3-D results once vibration is established. The reason is that the physical fluid motion becomes essentially 2-D, except for the wake turbulence, when VIV occurs; the vortices being shed have essentially a 2-D structure because of an increased wake correlation length.

The approach that we will take in this study is a 2-D LES calculation of the flow past a circular cylinder for $Re = 8000$ for a range of values of natural frequencies and damping ratios. The results to be presented are from a modified version of the method of Zhang and Dalton (1996). The present analysis will focus on calculating the cylinder oscillation and the influence of the natural frequency on the response. At resonance, the effect of both the mass of the cylinder and the material damping on the oscillation will be examined. The approach we will take is to set a value of the cylinder natural frequency and vary Re to determine the value of Re at which the maximum amplitude of oscillation will occur. Once this Reynolds number has been established, the cylinder natural frequency f_N is varied to examine the vibratory response at a fixed (calculated) value of the vortex shedding frequency f_{so} (for the stationary cylinder at the established value of Re).

2. Analysis

We will use the LES method to represent the wake turbulence at Re = 8000. The approach taken to calculate the flow field is the same as that of Zhang and Dalton (1996) with several notable differences to be described later. The finite-difference scheme serves as a natural filtering operation with a filter width that is the local grid size. The filtered 2-D governing equations are the Poisson equation for the stream function ψ,

$$\nabla^2\psi = -\omega \tag{1}$$

and the vorticity transport equation,

$$\frac{\partial\omega}{\partial t} + u\frac{\partial\omega}{\partial r} + \frac{v}{r}\frac{\partial\omega}{\partial\theta} = (\nu + \nu_t)\left(\frac{\partial^2}{\partial r^2} + \frac{1}{r}\frac{\partial}{\partial r} + \frac{\partial^2}{\partial\theta^2}\right)\omega, \tag{2}$$

where

$$u = \frac{1}{r}\frac{\partial\psi}{\partial\theta}, \quad \vartheta = -\frac{\partial\psi}{\partial r} \quad \text{and} \quad \omega = \frac{1}{r}\frac{\partial(rv)}{\partial r} - \frac{1}{r}\frac{\partial u}{\partial\theta}. \tag{3}$$

In the equations above, r and θ are the dimensional coordinates in the physical plane, t is the dimensional time, ν is the kinematic viscosity of the fluid, ν_t is the turbulent eddy viscosity, u and v are the radial and circumferential velocity components, and ω is the vorticity. All of the flow variables are the large-scale (resolvable) quantities.

The effects of the turbulence are represented by the eddy viscosity ν_t, which is determined by a subgrid scale model. In the present study, we use the Smagorinsky model,

$$\nu_t = (C_s\Delta)^2\sqrt{2S_{ij}S_{ij}}, \tag{4}$$

where C_s is the Smagorinsky constant, Δ is the length scale (taken here to be the local mesh size), and S_{ij} is the strain rate tensor.

We have selected the cylinder radius, R, and the steady approach velocity, U_∞, as the length and velocity scales, respectively, and the nondimensional time τ is tU_∞/R. The nondimensional governing equations are

$$\frac{\partial\omega}{\partial\tau} + u\frac{\partial\omega}{\partial r} + \frac{v}{r}\frac{\partial\omega}{\partial\theta} = \left(\frac{2}{\mathrm{Re}} + \frac{2}{\mathrm{Re}_t}\right)\nabla^2\omega \tag{5}$$

and

$$\nabla^2\psi = -\omega, \tag{6}$$

where

$$\nabla^2 = \frac{\partial^2}{\partial r^2} + \frac{1}{r}\frac{\partial}{\partial r} + \frac{\partial^2}{\partial\theta^2} \tag{7}$$

is the Laplacian operator. All of the terms in Eqs. (5)–(7) are now nondimensional. The Reynolds number and effective eddy Reynolds number are, respectively, $\mathrm{Re} = 2U_\infty R/\nu$ and $\mathrm{Re}_t = 2U_\infty R/\nu_t$. It is more convenient to solve this set of governing equations in a rectangular grid than a polar grid. Thus, the coordinate system is transformed to a rectangular system. The coordinate transformation, similar to the one used by Justesen (1991), is

$$r = 0.6\mathrm{e}^{\xi} + 0.4 \quad \text{and} \quad \theta = \pi\eta. \tag{8}$$

The physical and transformed planes are shown in Fig. 1.

We use the potential flow solution around a cylinder as the initial flow field. On the surface of the cylinder, the fluid velocity is equal to the velocity of the cylinder, i.e.,

$$v_t = \mathbf{v}\cdot\mathbf{t} \quad \text{and} \quad v_n = \mathbf{v}\cdot\mathbf{n}, \tag{9}$$

where v_t and v_n are, respectively, the tangential and normal components of the velocity of the cylinder, v is the fluid velocity vector, and $\mathbf{t}$ and $\mathbf{n}$ are, respectively, the unit tangent and normal vectors of the moving cylinder surface. In the coordinate system that is fixed on the cylinder, we have

$$v_t = v_n = 0 \tag{10}$$

or

$$\frac{\partial\psi}{\partial\xi}(1,\eta,\tau) = 0 \quad \text{and} \quad \psi(1,\eta,\tau) = 0. \tag{11}$$

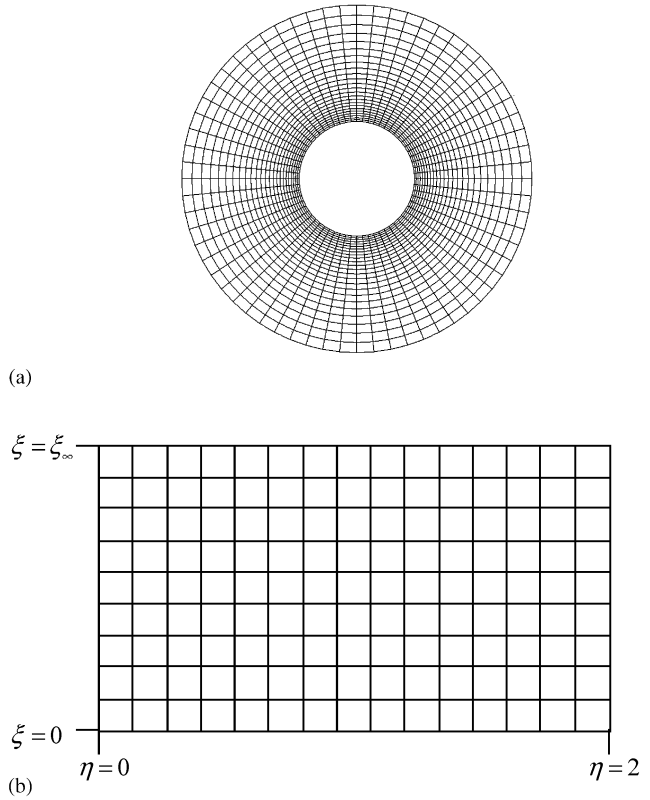

Fig. 1. (a) The physical domain with a nonuniform mesh in the radial direction and a uniform mesh in the circumferential direction. (b) Mesh system in the computational domain.

For the absolute coordinate system, we have

$$v_t \neq 0 \quad \text{and} \quad v_n \neq 0. \tag{12}$$

Neither velocity can be prescribed in advance. The Dirichlet part of the boundary conditions at infinity is taken to be

$$\psi(\xi_\infty, \eta, \tau) = \left(r(\xi_\infty) - \frac{1}{r(\xi_\infty)}\right)\left(U_\infty \sin \pi\eta + \frac{\mathrm{d}Y}{\mathrm{d}\tau}\cos \pi\eta\right) \quad \text{and} \quad \omega = 0, \tag{13}$$

where Y is the displacement of the cylinder ($Y = y/R$) relative to the at-rest position, $\mathrm{d}Y/\mathrm{d}\tau$ is the transverse velocity of the cylinder, and $r(\xi_\infty)$ is the radial distance to the outflow boundary. The nondimensional one-DOF equation for the vibratory motion of the cylinder is

$$\frac{\mathrm{d}^2 Y}{\mathrm{d}\tau^2} + 4\pi f_N \zeta \frac{\mathrm{d}Y}{\mathrm{d}\tau} + (2\pi f_N)^2 Y = \frac{1}{m^*\pi} C_L(\tau), \tag{14}$$

where ζ is the material damping ratio, f_N is the natural frequency, m^* is the ratio of the effective cylinder density to the fluid density (mass factor), and $C_L(\tau)$ is the instantaneous lift coefficient. The value of the instantaneous lift coefficient is determined from solving Eqs. (5) and (6) and then integrating the resulting pressure and shear stress distributions on the cylinder at each time level. The value of C_L at time τ is used in advancing the cylinder displacement to the next time level. Eq. (14) is used to advance the cylinder position to the time level $\tau + \Delta\tau$ using the known solution at time τ. Once the position is determined at the next time level, this new cylinder position and velocity are used as updated boundary conditions for solution of the LES equations. These equations are solved again to determine the lift and drag coefficients at the next time level. The process is repeated to determine cylinder positions and force descriptions at each new time level. Using this technique provides up-to-date information regarding the cylinder position and velocity. Thus,

the solution is advanced in time with the updated cylinder position and velocity providing the boundary conditions for the next time level.

The solution of the vibratory equation in the Zhang and Dalton results was a first-order correct method while the Newmark (1959) method used herein is essentially second-order correct. The earlier results of Zhang and Dalton method yielded a vibratory response that did not compare satisfactorily to experimental data for self-excited vibrations. As will be shown shortly, the present calculations give a more accurate comparison to experimental results.

3. Finite-difference representation

The governing equations and the initial and boundary conditions, Eqs. (5)–(13), are solved by a second-order accurate finite-difference scheme. Standard central differences are applied to all of the spatial derivatives. Upwinding differences are not used here because, in turbulent flows, the uncontrolled diffusion brought about by upwinding is better represented by the controlled diffusion of LES with subgrid scale models. The latter is based on the physical mechanism of turbulence and thus can better simulate the actual flows. The Poisson equation is solved efficiently by using a vectorized FFT algorithm. The Newmark method (1959) is used for time advancement of the cylinder oscillation from Eq. (14).

The differences between this study and that of Zhang and Dalton (1996) include a change in the outflow boundary condition, the size of the computational domain, the addition of a Van Driest model for wall damping, and a higher order extrapolation method to determine the wall vorticity. The new outflow boundary condition is a zero gradient condition (Neumann condition) for vorticity in the streamwise direction at the outflow boundary. Even though this condition is not quite correct physically, this method allows the outflow boundary to be transparent to the vortices crossing the boundary. Another advantage of this boundary condition is that it let the outflow boundary distance be decreased to five cylinder diameters as opposed to 25 as used by Zhang and Dalton. We chose the computational domain to be an O-grid with a radius of five cylinder diameters. The results of this assumption will be discussed in the following section. The computational grid should have a width of 10 diameters in the transverse direction to avoid blockage; so this radial distance of five diameters is also what is required to prevent blockage effects. The advantage of this size of computational domain is to have a finer grid system without an increase in the number of mesh points. This approach allows the LES method to be more representative of turbulence, especially at the outflow boundary where the physical grid size is large according to the transformation given by Eq. (8) (see O'Neil and Meneveau, 1997).

4. Results and discussion

Our approach to studying this VIV problem was to fix the natural frequency of the cylinder at $f_N = 0.1$ and run through a series of calculations to find at what value of Re the maximum amplitude of cylinder oscillation occurred. Once this Re value was determined, we then proceeded to vary the reduced velocity to determine how, at a fixed Reynolds number, changes in the natural frequency affect the vibratory response of the cylinder. For all of the calculations, the time step was 0.0025 and the grid size was 297×256 ($r \times \theta$) with the outer boundary five diameters from the cylinder center.

The use of a computational grid with a five-diameter extent is somewhat less than that which is typically used for such calculations. However, we feel that the use of the Neumann outflow boundary conditions (zero vorticity gradient) allows the solution to develop correctly. In Fig. 2, we show a comparison of the results on the cylinder surface for two different grids, one with a boundary distance of five diameters and one of eight diameters for a nonoscillating cylinder at $\mathrm{Re} = 13\,000$. The solution for the five-diameter domain is essentially the same as for the eight-diameter domain. The number of grid points for the eight-diameter domain is approximately twice that for the five-diameter domain. In addition, Fig. 3 shows the wake vortices for both domains; they are essentially identical to a distance of five diameters. This comparison validates the use of the Neumann outflow boundary condition and shows that a more compact domain can be used in the solution provided that the outflow boundary condition allows the flow to be represented properly as it passes the outflow boundary.

The Smagorinsky value of this modelling constant is $C_s = 0.18$. The value of C_s is actually not a constant, but is noted to have some dependence on the Reynolds number. The value of C_s used herein is essentially an average value and was determined from calculations at several different values of Re. We did not vary this value of C_s as the Reynolds number changed. Obviously, slightly different values of this modelling constant will produce slightly different results. However, determining precisely how the C_s value changes with Reynolds number would require calculations far more extensive than could be accommodated within this study.

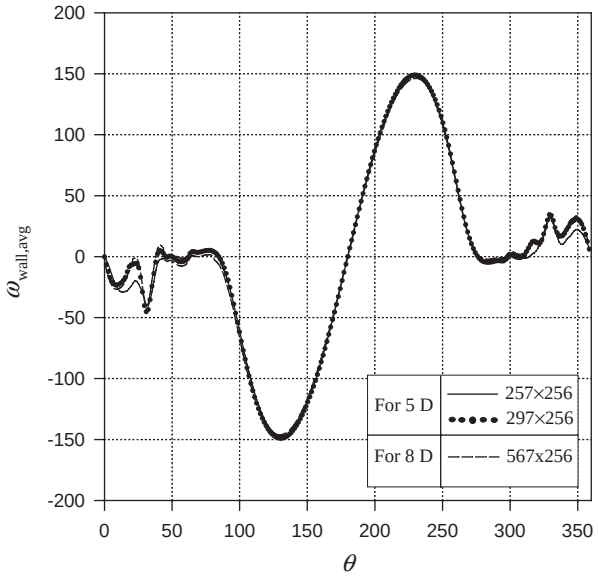

Fig. 2. Convergence comparison in the time-averaged wall vorticity between small and large domains for Re = 13 000.

Two different values of m^* (from Eq. (14)) were used, $m^* = 7.85$ and 1.67. The larger value represents a solid cylinder, which served as the main emphasis for this study, while the lower value represents a thin-walled water-filled cylinder. Both were taken to oscillate in water. Primary results will be presented for two material damping cases: $\zeta = 0.0$ and 0.02. In addition, three other values of ζ will be examined at resonance to determine the effect of material damping on the resonant behavior.

For purposes of validation, Fig. 4 shows the drag and lift coefficients plotted against time for a fixed circular cylinder at Re = 13 000. The time-averaged drag coefficient is about 1.28 ($\pm$0.3) compared to the experimental value of 1.2, while the lift coefficient had a range of $\pm$0.7 with an r.m.s. value of about 0.484. The experimental r.m.s. value of the lift coefficient at Re = 13 000 is about 0.43. The vortex-shedding frequency f_{so} that we calculated was 0.111 (Strouhal number of 0.222) whereas the experimental value is about 0.105 (Strouhal number of 0.21). The difference in $C_{Lr.m.s.}$ is significant (about 12%), but we attribute the difference between the calculated and experimental values of $C_{Lr.m.s.}$ to the fact that we are doing a 2-D calculation in a 3-D flow with perfect spanwise correlation of the shed vortices in the 2-D model.

Table 1 shows a comparison between our calculated 2-D and 3-D drag and lift coefficients and Strouhal number, some corresponding 3-D results from Lu et al. (1997) and those determined from experimental measurements for a fixed cylinder. At each value of Re, the calculated 2-D values of $\bar{C}_D$ exceed the experimental values, as expected. This is typical of a comparison of calculated 2-D drag coefficients and (3-D) experimental results. The $\bar{C}_D$ trend at lower values of Re is known to be about 5 to 10% high. Our $\bar{C}_D$ result at Re = 8000 is about 20% high. A reason for this was alluded to earlier. We used a constant value of C_s which was determined over a range of Reynolds numbers, but which was also the value at Re = 13 000. We chose to keep C_s constant instead of treating it as a variable, i.e., a function of Reynolds number. This approach will certainly lead to a numerical value for $\bar{C}_D$ that will have a nonconstant difference when compared to the experimental value over a range of Reynolds numbers. Again, the reason for this is that the (time-averaged) wake pressure is more negative for the 2-D representation because of the perfect spanwise correlation of vortex shedding. At higher values of Re, the 2-D calculated value of $\bar{C}_D$ is still too high, but the trend is not as uniform as at the lower values of Re. The 3-D results of Lu et al. (1997) show much better agreement with the experimental values because a more accurate representation of the wake dynamics is included.

Sarpkaya (1978) and Zdravkovich (1990) both suggest that the mass and damping parameters be considered independently in offshore applications. Khalak and Williamson (1999), however, have found a peak amplitude correlation with the mass-damping parameter ($m^*\zeta$) but they also suggest that m^* would be expected to influence the peak response independently under certain conditions. Govardhan and Williamson (2000) examined the VIV problem when the mass-damping parameter was relatively low, i.e., a value of 0.2 or less. The results of Feng (1968) were at $m^*\zeta$ values of slightly less than 1.0. As the value of $m^*\zeta$ decreases, Govardhan and Williamson found that the value of V_r, at which the maximum amplitude of oscillation occurs, increases.

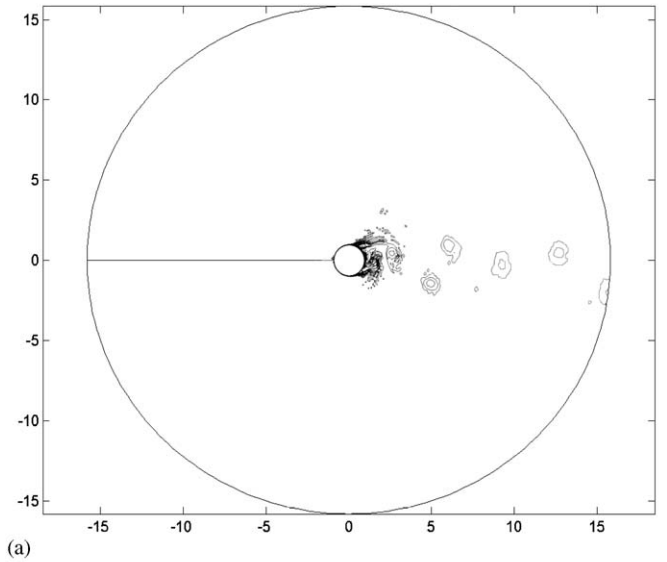

(a)

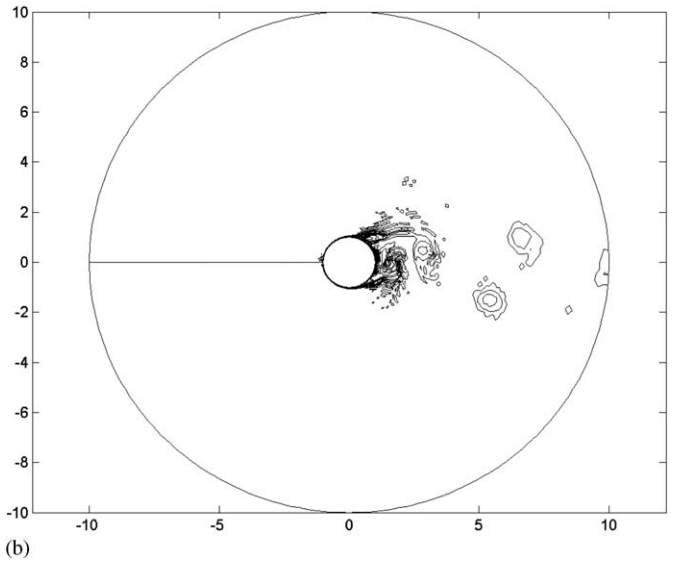

(b)

Fig. 3. Vorticity contours for a uniform flow past a fixed circular cylinder at Re = 13 000 with (a) 8-D-distance outflow boundary from the center point and (b) 5-D-distance outflow boundary from the center point.

By varying the value of Re from 2000 to 15 500, we found that the value of Re at which the maximum amplitude of oscillation (for $f_N = 0.1$) occurred was 8000. The VIV solutions, then, will be presented by taking the fixed cylinder vortex-shedding frequency f_{so} at Re = 8000 and varying the natural frequency f_N of the cylinder to form the frequency ratio (f_{so}/f_N). In a similar experimental investigation, the cylinder natural frequency would be fixed and the fluid velocity (i.e., the Reynolds number) would be changed to vary the frequency ratio. Our approach in changing the reduced velocity by varying the natural frequency eliminates any Reynolds number influence. However, we recognize that this approach is not likely in an experimental investigation because velocity is easier to change than the natural frequency.

Table 2 shows the maximum dimensionless displacement at several values of f_{so}/f_N at Re = 8000 with $m^* = 7.85$ and $\zeta = 0.02$. The trend is clear with the peak displacement occurring at $f_{so}/f_N = 1.233$ and falling off to small values at the extremes of the frequency ratio range $0.555 \leqslant f_{so}/f_N \leqslant 1.59$. All of the displacement plots show a beating behavior, as

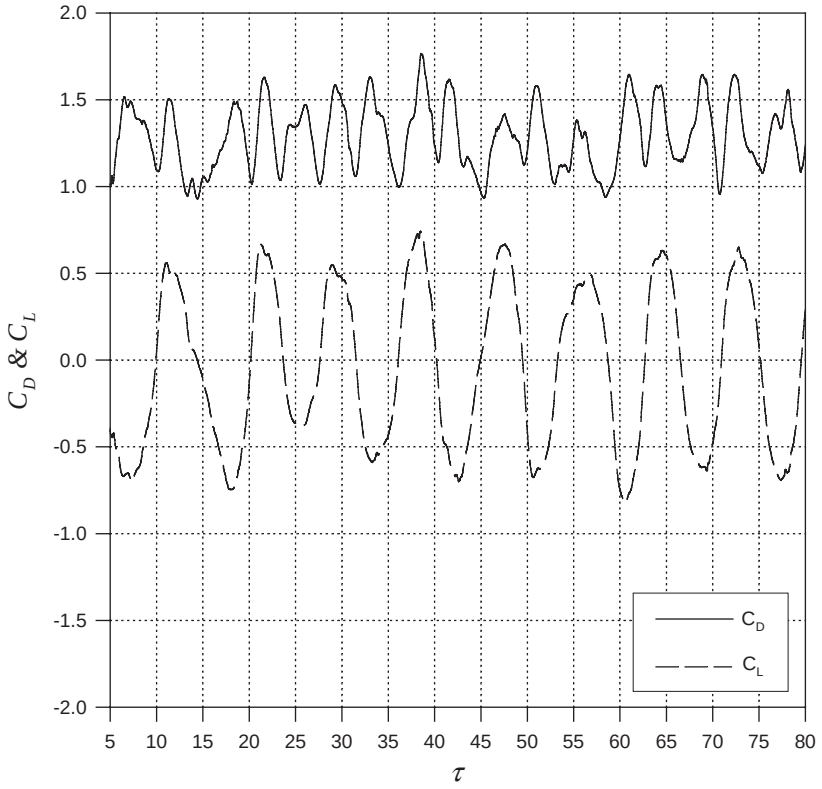

Fig. 4. C_D and C_L for a uniform flow past a fixed circular cylinder at Re = 13 000.

Table 1
Comparison of 2-D calculated values with 3-D and experimental values

Re	Calculated $\bar{C}_D$ (2-D)	Calculated $C_{Lr.m.s.}$ (2-D)	Calculated St (2-D)	Calculated* $\bar{C}_D$ (3-D)	Experimental $\bar{C}_D$	Experimental St
400	1.35	0.408	0.22		1.2	0.215
1000	1.3	0.386	0.233		1.0	0.21
3000				1.07	1.02	
8000	1.44	0.49	0.222		1.15	0.205
13 000	1.28	0.484	0.222		1.2	0.205
20 000				1.15	1.2	
44 200				1.18	1.2	

From Lu et al. (1997).

Table 2
Cylinder maximum displacement comparisons for $m^* = 7.85$ and $\zeta = 0.02$ at Re = 8000

V_r	Fixed	2.5	2.941	3.572	4.167	4.505	5.554	6.261	7.162
f_{so}/f_N		0.555	0.653	0.793	0.925	1.0	1.233	1.39	1.59
$(y/D)_{max}$	—	0.0265	0.053	0.17	0.215	0.25	0.3	0.2	0.08
$\bar{C}_D$	1.44	1.494	1.534	1.558	1.525	1.442	1.41	1.375	1.435
$C_{D,osc}$	±0.3	±0.35	±0.4	±0.6	±0.6	±0.6	±0.6	±0.55	±0.35
$C_{Lr.m.s.}$	0.49	0.558	0.66	0.805	0.786	0.593	0.335	0.365	0.35
$C_{L,osc}$	±0.7	±0.8	±1.0	±1.6	±1.6	±1.5	±0.6	±0.7	±0.6

seen in Fig. 5 for $f_{so}/f_N = 0.793$, except at the extremes of the frequency range. This beating phenomenon was observed by Feng (1968) in air and by Sarpkaya (1978) and Khalak and Williamson (1999), both in water. As will be shown later, the presence of beating is controlled by the value of ζ, the material damping ratio, used in the calculation. This comment is somewhat verified, as shown in Fig. 5, where results for values of $\zeta = 0.0$ and 0.02 are shown with the larger amplitude occurring for the case with no material damping. Fig. 6 shows the clear lock-on region for the case of $m^* = 7.85$. We notice how this region is getting wider as the damping ratio decreases. From Table 2, we also notice a significant increase in the values of $C_{Lr.m.s.}$ at the beginning of the lock-on and a decrease as perfect synchronization is being approached. Sarpkaya (1978) has addressed this trend in C_L behavior. In addition, the drag fluctuations are increasing with oscillations. Figs. 7 and 8 show the profiles of the calculated drag and lift coefficients at $f_{so}/f_N = 0.925$ and 1.233. From the values shown in Table 2, the effect of the frequency ratio on the extent of cylinder oscillation (i.e., VIV) is quite evident. The peak oscillation occurs at $f_{so}/f_N = 1.233$ which corresponds to a reduced velocity ($V_r = U_\infty/f_N D$) value of about 5.5.

The effect of changing values of ζ is presented by results shown in Fig. 9. Response of the oscillation to increasing values of material damping at $m^* = 7.85$ is quite evident from the values in Fig. 9. Increasing ζ from 0.0 to 0.1 produced a 64% decrease in maximum amplitude of oscillation while an increase in ζ from 0.02 to 0.1 produced a decrease of about 56%. This peak amplitude continues to decrease as ζ increases, accompanied by a decrease in the beating behavior. Also, the period of the imposed higher harmonics becomes greater with increased damping because damping

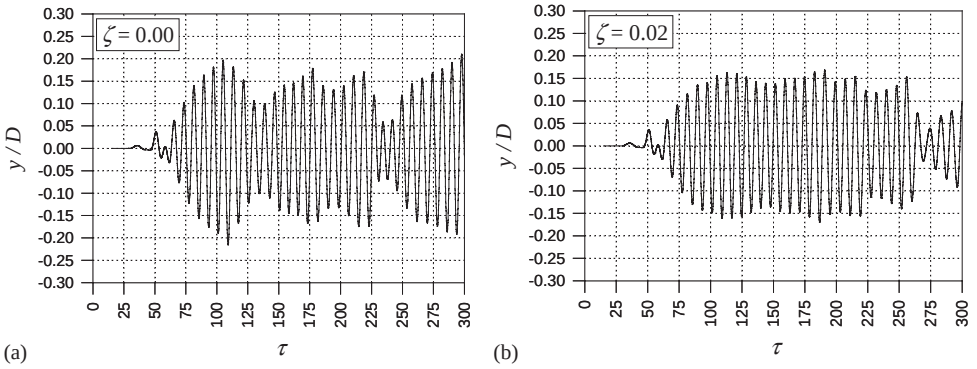

Fig. 5. Effect of ζ on the beating phenomenon of a vibrating solid circular cylinder with $f_N = 0.14$ at Re = 8000. (a) $\zeta = 0.00$, (b) $\zeta = 0.02$.

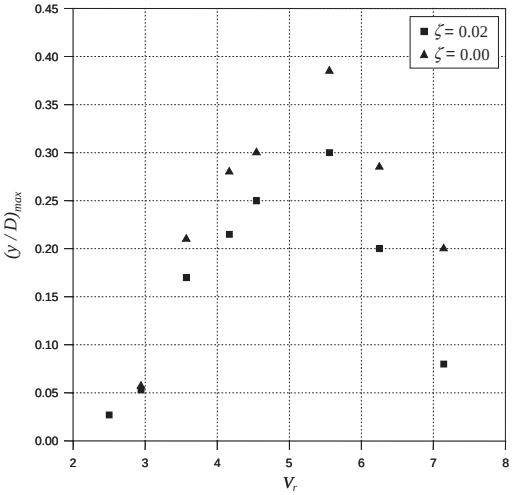

Fig. 6. Maximum transverse amplitudes in the lock-on region for a vibrating solid circular cylinder with two different damping ratios at Re = 8000.

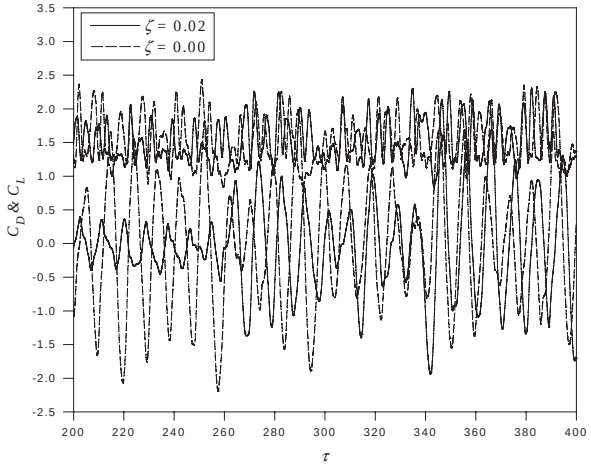

Fig. 7. C_D and C_L for a uniform flow at Re = 8000 past a vibrating solid circular cylinder with $f_N = 0.12$ and two different damping ratios.

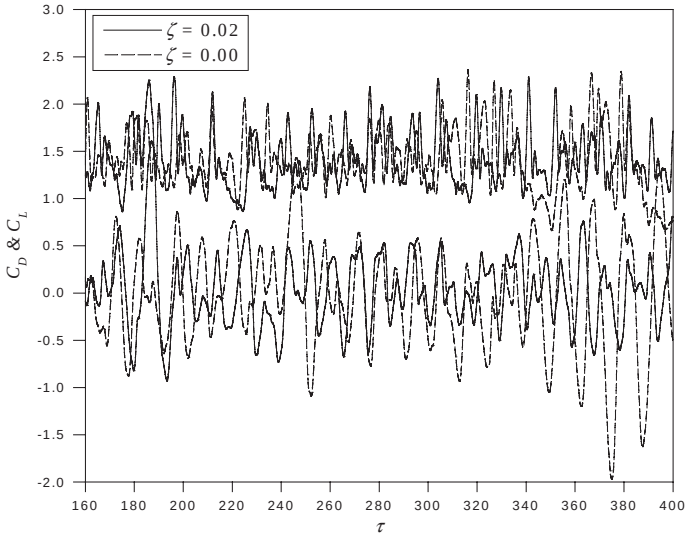

Fig. 8. C_D and C_L for a uniform flow at Re = 8000 past a vibrating solid circular cylinder with $f_N = 0.09$ and two different damping ratios.

tends to diminish the low frequency effects. Fig. 10 shows the cylinder oscillation at $\zeta = 0.1$ (and $m^* = 7.85$); note the significant decrease in beating, especially in contrast to Fig. 5 for $\zeta = 0.02$. The beating becomes less pronounced as the value of ζ is increased, but the contrast is shown only for $\zeta = 0.02$ and 0.1 (compare Figs. 5 and 10).

Listed in Table 3 are the results from the VIV calculations for $m^* = 1.67$. The effect of decreasing the value of m^* is to increase the magnitude of the forcing function on the right-hand side of Eq. (14). This increase drives the oscillation to higher amplitudes. Fig. 11 shows the maximum peak variation with V_r. From the behavior of the lock-on region, it is not clear that this simulation is capable of detecting the three branches of the lock-in region (initial, upper and lower branches) as addressed in Govardhan and Williamson (2000). There is a discrepancy in what seems to be our lower branch in that it does not have a constant-value behavior. The reason behind this discrepancy is likely related to the manner in which we vary V_r (i.e., by changing f_N) which becomes unrepresentative for $V_r > 13.0$. Fig. 12 shows that the cylinder oscillation frequency (f_c) is very low for $V_r > 13.0$. This can be explained by the cylinder having a diminishing stiffness as V_r increases, with the stiffness becoming quite small for values of $V_r > 13.0$. Another discrepancy is that the

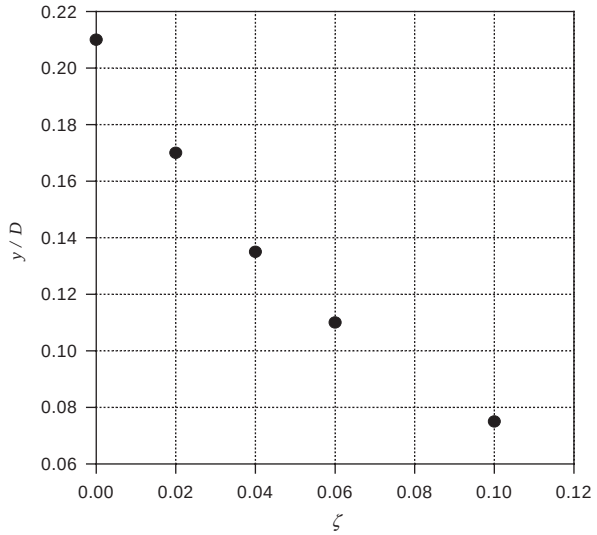

Fig. 9. Effect of material damping ratio on the maximum peak amplitude of a vibrating solid circular cylinder with $f_{so}/f_N = 0.793$ and $m^* = 7.85$ at Re = 8000.

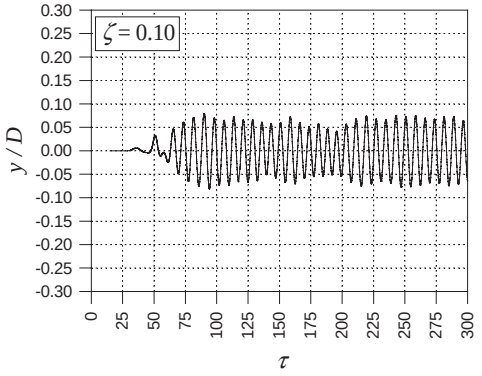

Fig. 10. Effect of high material damping ratio ($\zeta = 0.1$) on the beating phenomenon of a vibrating solid circular cylinder with $f_N = 0.14$ at Re = 8000.

Table 3
Cylinder maximum displacement comparisons for $m^* = 1.67$ and $\zeta = 0.02$ at Re = 8000

V_r	2.5	3.572	5.554	7.162	10	13.153	16.67	20	22.75
f_{so}/f_N	0.555	0.793	1.233	1.59	2.22	2.92	3.7	4.44	5.05
$(y/D)_{\max}$	0.21	0.418	0.784	0.824	0.873	0.64	0.87	0.71	0.66
$\bar{C}_D$	1.6767	1.4774	1.938	1.3913	1.3709	1.3488	1.3215	1.3576	1.384
$C_{L\text{r.m.s.}}$	1.0143	0.9453	0.939	0.4083	0.2345	0.2054	0.2038	0.1883	0.2048

ratio of f_c/f_N, during lock-in, is slightly less than one which can be interpreted by the forcing function used by Govardhan and Williamson (2000) being a regular sinusoidal function and the fluid damping is considered to have a constant value. In our study, the forcing function is irregular and the fluid damping is implicitly calculated in the fluid forces which makes it vary with time.

In Fig. 13, the near wake behavior is shown for different times in one and one-half oscillatory cycles at $f_{so}/f_N = 1.233$, $\zeta = 0.02$, and $m^* = 7.85$. These results clearly show the near wake response to the oscillation. As the cylinder moves

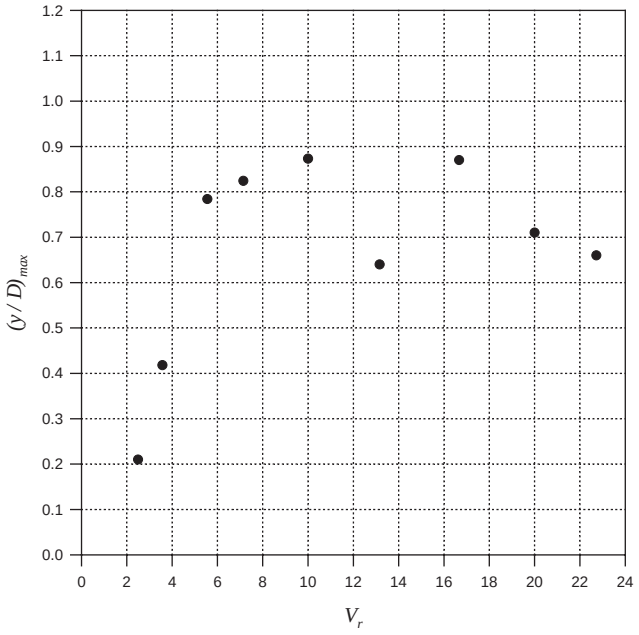

Fig. 11. Maximum transverse amplitudes in the lock-on region for a vibrating thin-walled water-filled circular cylinder with $\zeta = 0.02$ at Re = 8000.

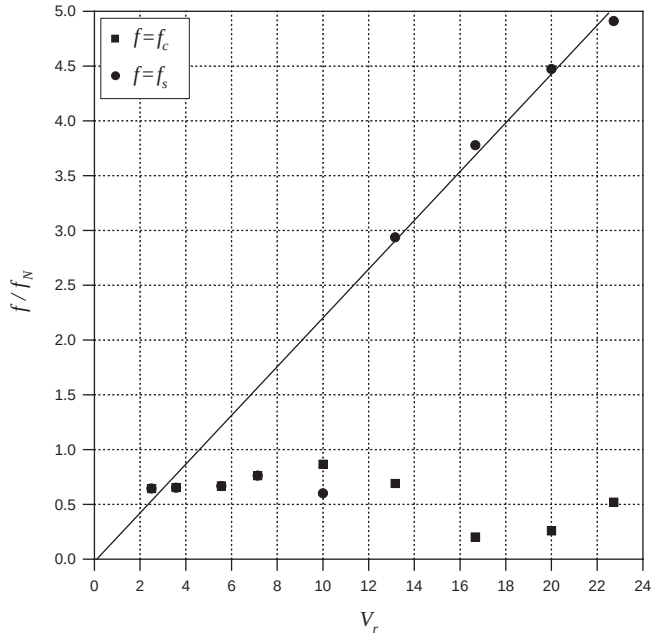

Fig. 12. Shedding and vibration frequencies behavior in the lock-on region for a vibrating thin-walled water-filled circular cylinder with $\zeta = 0.02$ at Re = 8000.

upward in the vibratory cycle, the near wake is expected to be deflected down from the center-line, with the converse being true for the cylinder moving down in the cycle. This aspect of the near wake behavior is evident in the calculated results.

The wake response results we have found do not fit in the 2S, 2P, etc. mode descriptions of Williamson and coworkers. There are several reasons why this disagreement might exist. The maximum Re value of Govardhan and

Williamson (2000) was 3700 while ours is 8000. In Govardhan and Williamson, they state (p. 91) that, at higher Re ($\cong 5000$), the flow visualization technique is "somewhat unclear". This can only mean that the existence of modes such as 2S and 2P is not yet established beyond Re = 3700. Not that our Reynolds number is sufficiently high (Re = 8000), but it certainly is larger than that of Govardhan and Williamson (Re = 3700). Zdravkovich (1997), in his book on flow past a cylinder, summarizes the early work of Gerrard and Bloor regarding the wake of a cylinder and the development of wake turbulence. The wake turbulence begins at about Re = 200 with the shear layers remaining viscosity dominated. The shear layers begin to develop instabilities at Re ~ 1300. By Re ~ 11 000–13 000, the shear layers have become fully turbulent. In fact, this is what accounts for the jump in the steady flow drag coefficient at Re ~ 11 000–13 000. The transition point on each shear layer has moved forward to the separation point which causes a slight increase in pressure drag. At these lower values of Re (3700 and even 8000), the physical shear layers are transitional and the wake structure is still developing. The LES method, at the present time, does not seem to have the capability to examine this transitional nature of turbulence generation in the shear layer. Thus, it seems that there is an obvious Reynolds number effect that is present in the formation of the wake vortices. This statement is supported by the PIV studies of Lin et al. (1995) who compare near wake PIV images at Re = 1000, 5000, and 10 000 and the flow visualization studies of Dalton et al. (2001) who compare flow visualization results at Re = 1000 and 3000, among others. There are obvious Reynolds number effects that are shown in the results of these two studies. This wake-transition situation is even more pronounced for the VIV case because of the time-dependence in the shear layers. We support the position of Govardhan and Williamson that the vortex modes are unclear at higher Reynolds numbers. Our results do not show the 2S, 2P, etc., type of modes at Re = 8000. We suspect that these modes are descriptive of the flow at lower values of Re and for sinusoidal oscillations. At values of Re as high as 8000, we suggest that these modes that are so descriptive of the VIV wakes at much lower values of Re are no longer present (perhaps in a recognizable form) and the wake structure has more of a similarity to that of the nonoscillating cylinder. Govardhan and Williamson continue to discuss this wake-mode behavior in p. 108. They note that several CFD investigators have not found the 2P mode to be present where it is expected based on the earlier work of Williamson and Roshko (1988). In Blackburn et al. (2001), it is speculated that 2-D low Reynolds number simulations are not sufficient to capture the 2P modes that are attributable to 3-D effects. Our calculations are also 2-D, but we feel that there are other reasons for the lack of agreement with the standard mode observations. Govardhan and Williamson note that their results indicate that "the apparent disparity between the high Reynolds number experiments (Re ~ 2000–4000) and the simulations seems to be a Reynolds number effect". We fully support these statements and further suggest that, based on our CFD results, albeit 2-D, the wake structure has a continuing dependence on the Reynolds number. A clear understanding of the dependence remains to be found and is just a small part about what remains to be discovered about VIV.

Another comment on the 2S, 2P, etc. mode description is that the existence of these structures and their relation to cylinder oscillation was established for sinusoidal oscillations. When the oscillation is not purely sinusoidal (as in the results herein and also in those of Blackburn et al.), the 2S, 2P, etc. structures may not become fully established because the amplitude of oscillation and the phase angle are both time dependent. The lack of a constant amplitude suggests that the vortex structures do not have the same size or extent that they would have for a constant amplitude oscillation. The lack of constancy in amplitude and phase angle could quite likely lead to the lack of repeatability in vortex formation which certainly could suppress the standard mode patterns. This issue also needs further study.

In addition to the nonconstant amplitude contributing to the expected lack of agreement with the 2S, 2P, etc. structures, we also note that another source of conflict is present. Our calculations are done at a constant Reynolds number; we changed the reduced velocity by changing the natural frequency, not the velocity itself. The traditional 2S, 2P behaviors were observed for a given natural frequency and the reduced velocity was increased by increasing the velocity. This increase in velocity imposed a Reynolds number effect on these earlier results which is absent in our case.

In both the forced oscillation and the self-excited cases studied by Williamson and coworkers, a constant phase angle between the displacement and the force was typically assumed and found. We do not agree that a direct comparison can be made between the forced oscillation and self-excited oscillation cases, especially when the self-excited case is not sinusoidal. Our calculations produced a nonsinusoidal response and did not yield a constant phase angle. In fact, the numerical study of Blackburn et al. (2001) also did not yield a constant phase angle. The numerical simulation of Blackburn et al., similar to ours, seems to produce a nonsinusoidal oscillation. Their simulation also does not assume that a constant phase angle exists and does not yield one.

The wake vorticity plots in Fig. 13 depict a typical wake structure for a self-excited oscillation. This illustration represents about one and one-half oscillations. Recall that the cylinder motion is oscillatory, but not sinusoidal. At $\tau = 140$, the flow/oscillation combination has produced a pair of relatively symmetric vortices in the near wake. The implication of this pattern is that no vortices are being shed for a relatively short time which means that the vortices that were shed at a slightly earlier time have passed out of the computational grid. As time progresses, the wake again

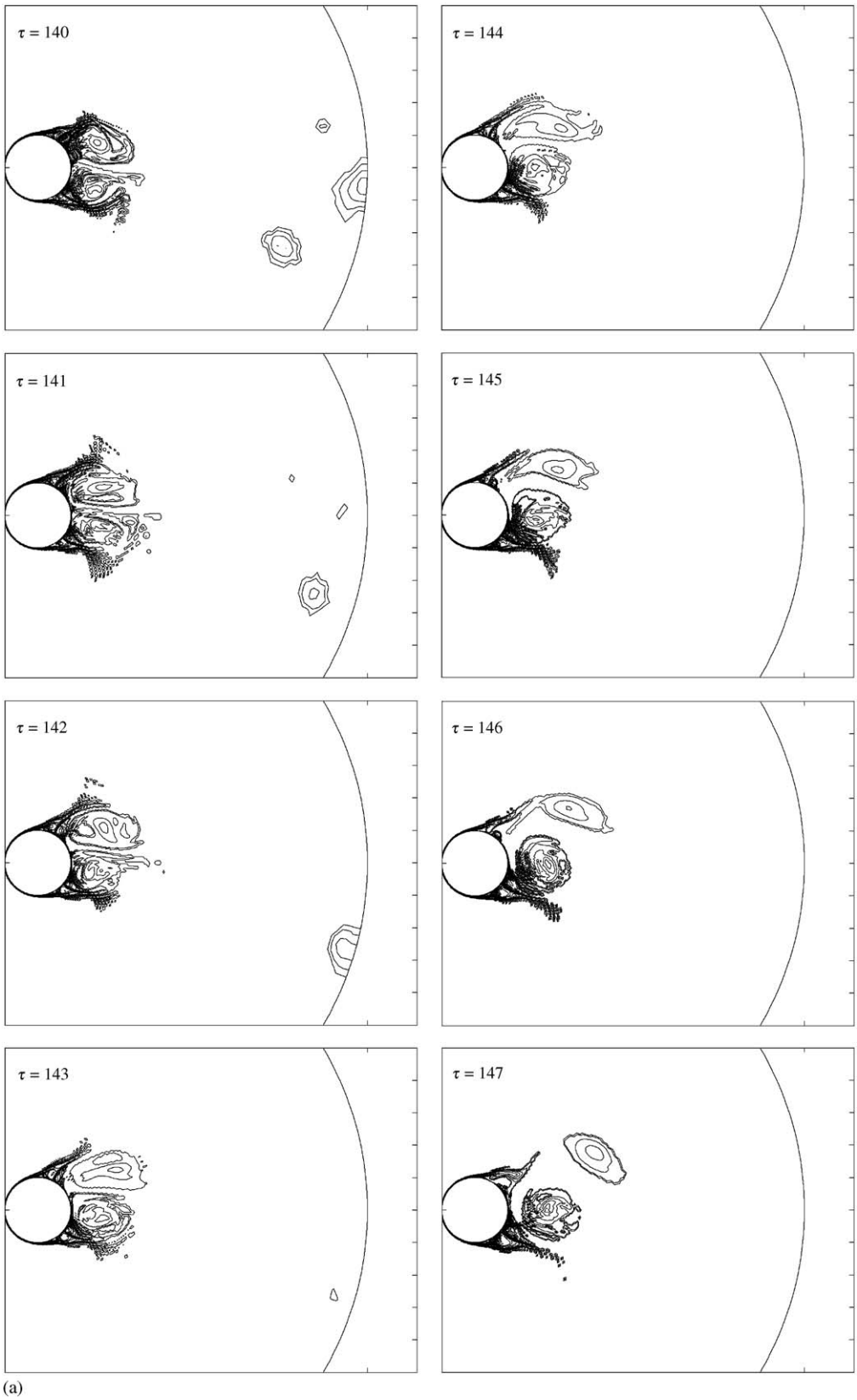

(a)

Fig. 13. Physical vorticity contours of a vibrating solid circular cylinder over one and one-half cycles with $f_N = 0.09$ and $\zeta = 0.02$ at $\mathrm{Re} = 8000$.

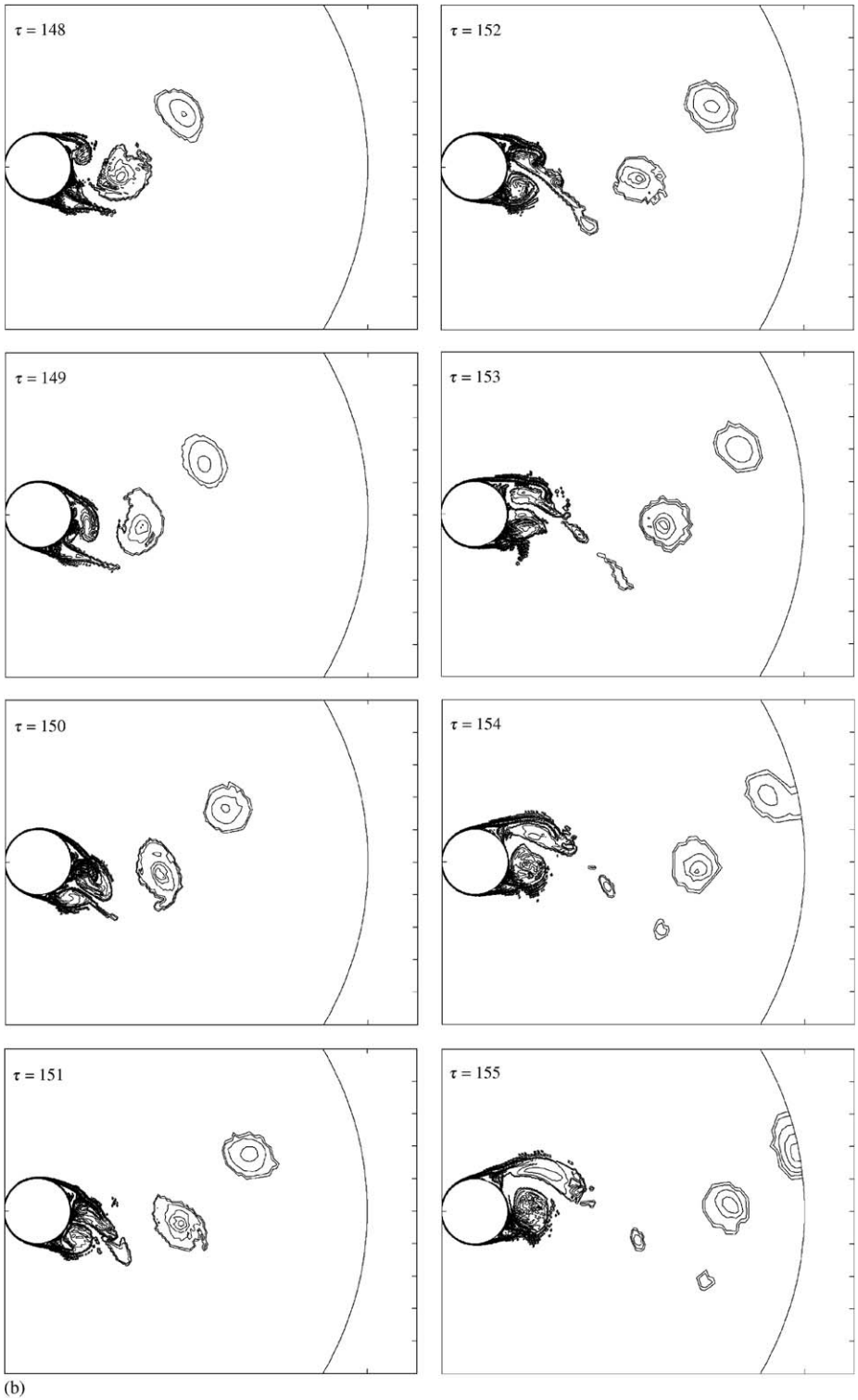

(b)

Fig. 13 (*continued*).

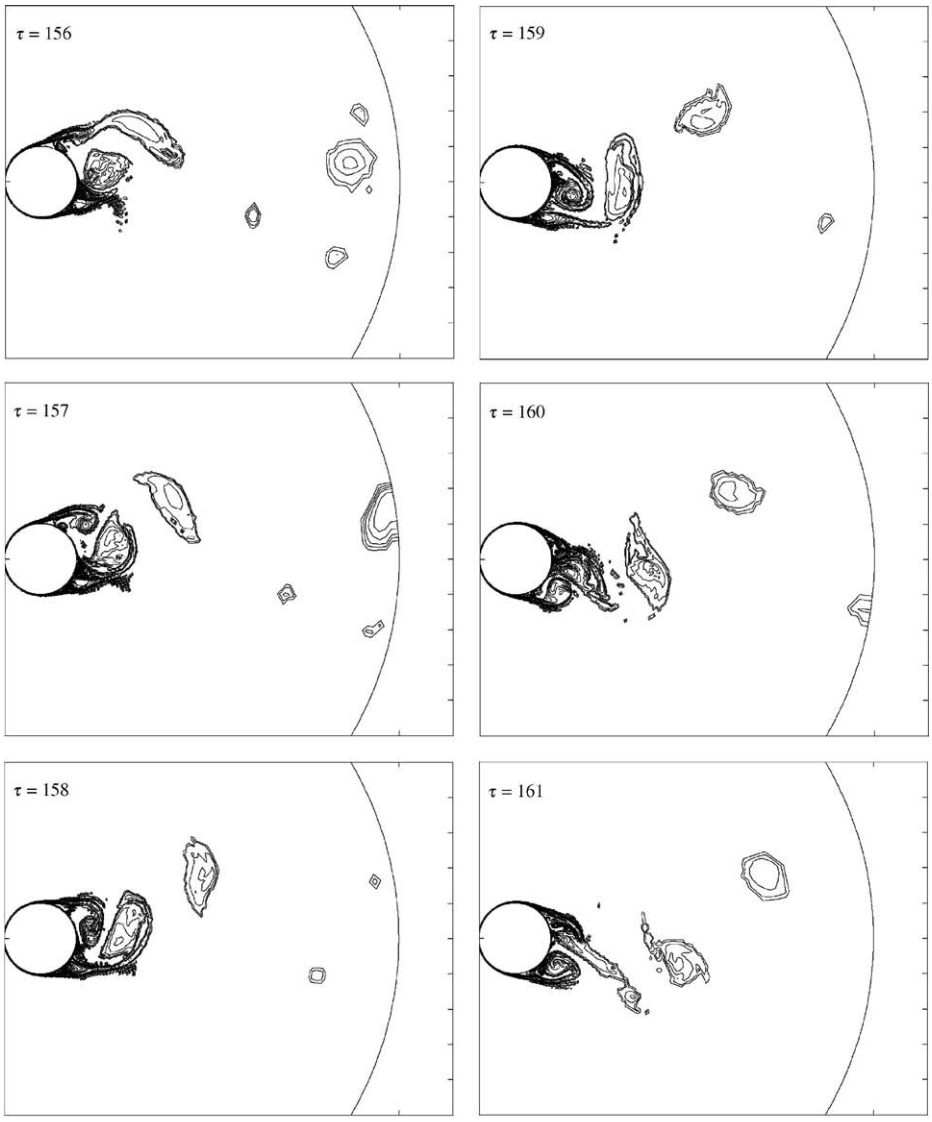

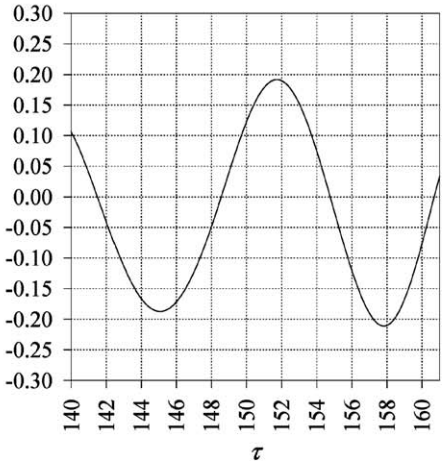

(c)

Fig. 13 (*continued*).

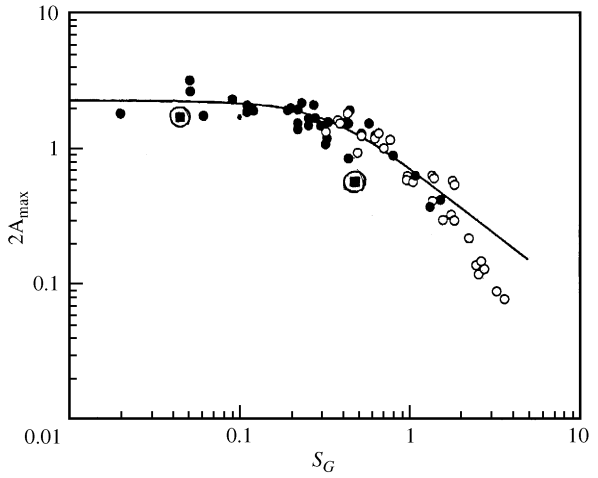

Fig. 14. Griffin "universal" plot showing where our calculations, indicated by ■, compared to the Skop–Balasubramanian correlation and the data compiled by Griffin. The figure is from Skop and Balasubramanian (1997).

becomes asymmetric and, at $\tau = 147$, shedding has again become established. This representation is carried through $\tau = 161$ during which interval the process of periodic shedding for the oscillating cylinder has become re-established.

The vorticity plots for the oscillating cylinder (Fig. 13) contain some noise that is a function of the range of vorticity values selected for the plot. By tightening this range of values, a much smoother appearing wake structure can be represented. We suggest that part of this noise problem is that this calculation is at $\mathrm{Re} = 8000$. There are very few calculations that show the vorticity plots at a Reynolds number this high. We are aware of only one PIV study at values of Re as high as those in this study or in several other computational studies (see Lin et al., 1995). In the study by Tutar and Holdo (2000), fairly smooth vorticity contours were obtained at $\mathrm{Re} = 2.4 \times 10^4$. Tutar and Holdo used an outflow boundary distance of 15-D, but used about one-half the number of mesh points than we used for the calculation involving a 5-D distance. Based on the calculations we have performed in this and earlier studies, it is not clear that the grid resolution employed by Tutar and Holdo is sufficient to describe this problem adequately.

Fig. 14 shows the results of our calculations plotted on Griffin's "universal" amplitude vs. mass-damping curve. This plot is from Skop and Balasubramanian (1997) and includes the Skop–Balasubramanian correlation as well as data collected by Griffin and others. Our results at $m^* = 1.67$ agree reasonably well with the data in the Griffin plot, but are a bit below the Skop–Balasubramanian correlation. At $m^* = 7.85$, our results fall about 40% below the correlation and about 10% below the data.

5. Conclusions

Two-dimensional calculations of the self-excited response of a circular cylinder to a uniform flow are shown to be a reasonably accurate representation of the VIV problem. In spite of the shortcomings of a 2-D representation, the results show the expected vibratory response of the cylinder for $0.555 < f_{so}/f_N < 1.59$. Calculations were done for two values of the mass factor m^* ($m^* = 1.67, 7.85$), and several values of ζ ($0.0 \leqslant \zeta \leqslant 0.1$). Calculations at values of the mass-damping factor of 0.0333 and 0.157 were done in detail. The cylinder was shown to follow the expected VIV response at $m^*\zeta = 0.157$ with lock-on shown to be present in a vivid and expected manner, peaking at a reduced velocity of about 5.5. At $m^*\zeta = 0.0333$, the results of the calculations are consistent with experimental values which show a broadband of VIV responses at this value of the mass-damping factor. The phenomenon of beating was examined and was found to be reduced significantly by an increase to a value of 0.1 for the material-damping ratio. We did not observe the standard modes of vortex shedding which have been observed by several investigators, primarily for the forced-oscillation problem. There are at least three possible explanations for this discrepancy: The first is that this was a calculation at a value of Re large enough not to have been examined in regard to the existence of these standard modes that have been established for lower values of Re. The second, and probably more likely, is that the oscillation calculated herein is not sinusoidal which would interfere with the timing and length of the vortex structures and influence the overall wake

structure in that manner. A third, and equally probable reason, is that our results are at a constant Reynolds number whereas the experimental results for which these standard patterns of vortex structures were observed are not at constant Reynolds number.

Acknowledgements

Dexter Hill of NEC Systems, Inc. provided computer time on the SX4 machine at the NEC facility in The Woodlands, TX. We are grateful to Dexter Hill for the computer time that made this effort possible. We are grateful to Jeff Zhang for several helpful discussions. The code used in this effort had its basis in the code used in the Zhang and Dalton (1996) paper. We have made a number of modifications in the code in order to do these calculations. The first author thanks the Fulbright Commission for the graduate fellowship that allowed him to come to the US. He is also grateful to the American Association of Drilling Engineers for his present graduate fellowship which is now in its second year.

References

Bearman, P.W., 1984. Vortex shedding from oscillating bluff bodies. Annual Review of Fluid Mechanics 16, 195–222.

Blackburn, H.M., Govardhan, R., Williamson, C.H.K., 2001. A complementary numerical and physical investigation of vortex-induced vibration. Journal of Fluids and Structures 15, 481–488.

Breuer, M., 1999. A Challenging test case for Large Eddy Simulation: high Reynolds number circular cylinder flow. Proceedings of the Turbulence and Shear Flow Phenomena-1, Santa Barbara, CA, September.

Dalheim, J., 1999. Numerical prediction of VIV on deepwater risers subject to shear currents and waves. Paper No. 10933, Offshore Technology Conference, Houston.

Dalton, C., Xu, Y., Owen, J.C., 2001. Suppression of lift on a circular cylinder due to vortex shedding at moderate Reynolds numbers. Journal of Fluids and Structures 15, 617–628.

Evangelinos, C., Lucor, D., Karniadakis, G.E., 2000. DNS-derived force distribution on flexible cylinders subject to vortex-induced vibration. Journal of Fluids and Structures 14, 429–440.

Feng, C.C., 1968. The measurement of vortex-induced effects in flow past stationary and oscillating circular and D-section cylinders. M.A.Sc. Thesis, University of British Columbia, Vancouver.

Govardhan, R., Williamson, C.H.K., 2000. Modes of vortex formation and shedding response of a freely vibrating cylinder. Journal of Fluid Mechanics 420, 85–130.

Gu, W., Chyu, C., Rockwell, D., 1994. Timing of vortex shedding from an oscillating circular cylinder. Physics of Fluids 6, 3677–3682.

Guilmineau, E., Queutey, P., 2001. Numerical simulations in vortex-induced vibrations at low mass-damping. AIAA paper number 2001–2852, Anaheim, June 2001.

Herjford, K., Drange, S.O., Kvansdal, T., 1999. Assessment of vortex-induced vibration on deepwater risers by considering fluid–structure interaction. ASME Journal of Offshore Mechanics and Arctic Engineering 121, 207–212.

Jordan, S.A., Ragab, S.A., 1998. A Large Eddy Simulation of the near wake of a circular cylinder. Journal of Fluids Engineering 120, 243–252.

Justesen, P., 1991. A numerical study of oscillating flow around a circular cylinder. Journal of Fluid Mechanics 222, 157–196.

Khalak, A., Williamson, C.H.K., 1999. Motions, forces, and mode transitions in VIV at low mass damping. Journal of Fluids and Structures 13, 813–851.

Kravchenko, A.G., Moin, P., 2000. Numerical studies of flow over a circular cylinder at $Re = 3900$. Physics of Fluids 12, 403–417.

Lecointe, Y., Piquet, J., 1989. Flow structure in the wake of an oscillating cylinder. Journal of Fluids Engineering 111, 139–148.

Lin, J.C., Towfighi, J., Rockwell, D., 1995. Instantaneous structure of the near wake of a circular cylinder: on the effect of the Reynolds. Journal of Fluids and Structures 9, 409–418.

Lu, X., Dalton, C., 1996. Calculation of the timing of vortex formation from an oscillating circular cylinder. Journal of Fluids and Structures 10, 527–541.

Lu, X., Dalton, C., Zhang, J., 1997. Application of Large Eddy Simulation to flow past a circular cylinder. ASME Journal of Offshore Mechanics and Arctic Engineering 119, 219–225.

Majumdar, S., Rodi, W., 1985. Numerical calculations of flow past circular cylinders. Proceedings of the Third Symposium on Numerical and Physical Aspects of Aerodynamic Flows, Long Beach, CA.

Newmark, N.M., 1959. A method of computation for structural dynamics. Journal of the Engineering Mechanics Division of ASCE 85, 67–94.

O'Neil, J., Meneveau, C., 1997. Subgrid-scale stresses and their modeling in a turbulent plane wake. Journal of Fluid Mechanics 349, 253–293.

Ongoren, A., Rockwell, D., 1988. Flow structure an oscillating cylinder. Part 1: mechanisms of phase shift and recovery of the near wake. Journal of Fluid Mechanics 191, 197–223.

Saltara, F., Meneghini, J.R., Sigueira, C.R., Bearman, P.W., 1998. The simulation of vortex shedding from an oscillating circular cylinder with turbulence modeling. Paper No. 13, Proceedings of the ASME Conference on Bluff Body Wakes and Vortex-Induced Vibrations, Washington, DC, June.

Sarpkaya, T., 1978. Fluid forces on oscillating cylinders. ASCE Journal of Waterway, Port, Coastal, and Harbors 104, 275–291.

Sarpkaya, T., 1979. Vortex-induced oscillations. Journal of Applied Mechanics 46, 241–258.

Skop, R.A., Balasubramanian, S., 1997. A new twist on an old model for vortex-excited vibrations. Journal of Fluids and Structures 11, 395–412.

Tutar, M., Holdo, A.E., 2000. Large Eddy Simulation of a smooth circular cylinder oscillating normal to a uniform flow. ASME Journal of Fluids Engineering 122, 694–702.

Williamson, C.H.K., Roshko, A., 1988. Vortex formation in the wake of an oscillating cylinder. Journal of Fluids and Structures 2, 355–381.

Yamamoto, C.T., Saltara, F., Martins, C.A., Meneghini, J.R., Ferrari, J.A., 2001. Hydroelastic response of offshore risers using CFD. Paper No. OFT-1052, Proceedings of the OMAE, Rio De Janeiro, Brazil, June.

Zdravkovich, M.M., 1990. On origins of hysteretic response of a circular cylinder induced by vortex shedding. Zeitschrift fur Flugwissenschaften Weltramforschung 14, 47–58.

Zdravkovich, M.M., 1997. Flow Around a Circular Cylinder. Oxford University Press, Oxford.

Zhang, J., Dalton, C., 1996. Interaction of vortex-induced vibrations of a circular cylinder and a steady approach flow at a Reynolds number of 13,000. Computers and Fluids 25, 283–294.

Zhang, J., Dalton, C., 1997. Interaction of a Steady approach flow and a circular cylinder undergoing forced oscillation. ASME Journal of Fluids Engineering 119, 808–813.

Zhou, C.Y., So, R.M.C., Lam, K., 1999. Vortex induced vibrations of an elastic circular cylinder. Journal of Fluids and Structures 13, 165–189.